Fuel cell electrocatalsis : oxygen reduction on Pt-based nanoparticle catalysts

Vliet, D.F. van der

Chapter 8

Electrochemistry of Pt (100) in Alkaline Media: A Voltammetric Study

Pt (100) is one of the fcc metal surface planes that reconstruct upon annealing at high temperatures. The state of the surface is important in electrochemistry, in order to correlate catalytic behavior with surface structure. Therefore, the behavior of single crystalline Pt (100) in alkaline media was investigated, with particular attention paid to surface long range order. It was found that, in line with previous results, the manner of cooling the crystal after annealing influenced the state of surface significantly, with a profound effect on blank cyclic voltammetry as well as on carbon monoxide oxidation. Different ratios of inert and reductive gases were used to see if an optimal mixture could be obtained. Using air, argon, hydrogen, CO, and combinations of these gases gave rise to different states of the surface, with clear observable differences in blank voltammetric behavior and CO stripping. Also, the effect of alkali-metal cations and bromide on the blank and CO stripping voltammetry was investigated. Our main conclusion is that cooling in a carbon monoxide containing gas gives a clean, almost defect-free surface with long-range 1x1 symmetry. A similar surface can also be prepared with a hydrogen-containing cooling gas, but the content of hydrogen in that stream is critical.

The contents of this chapter have been accepted: D. van der Vliet and M.T.M. Koper, *Surf. Sci.* **(2010),** DOI: 10.1016/j.susc.2010.07.027

8.1 Introduction

For many decades now, single crystalline electrodes have been successfully used in surface electrochemistry, in an effort to correlate catalytic behavior with surface morphology. Especially the basal planes of the most dominant catalytic metal, platinum, have been used extensively in the literature. To understand catalytic trends, knowing the physical state of the surface is of utmost importance, which is why many surface sensitive techniques such as STM have been of valuable use in electrochemistry. [1-3]

On the three low-index planes of Pt, the (100) plane often exhibits the highest catalytic activity, especially for bond-making and bond-breaking reactions. [4-12] Therefore, reliably preparing a (100) surface with long-range order is key to understanding structure sensitivity in electrocatalysis. However, Pt (100) is considered to be a difficult surface to prepare in electrochemistry, reproducibility generally being an issue. From vacuum studies, it is known that Pt (100), as well as Pt (110) form reconstructed surfaces upon annealing [7, 8, 13-22]. This reconstruction can be lifted when the electrode is cooled in H_2, CO or NO. [7, 22, 23] Electrochemical studies confirmed that the reconstruction is (partially) retained, even if the crystal is transferred to an electrochemical cell, in contact with acid electrolyte [23-25]. For alkaline media, many different reports in which Pt (100) was used have been published. [4, 10, 26-33] In these papers, the blank cyclic voltammetry (CV) is not well defined; compare for example [10, 27] with [4, 28], in which the blank CVs look significantly different. This reinforces the belief that Pt (100) is a difficult surface to work with. In all reports, the CV exhibits four features on both the positive and the negative scan between 0.2V and 0.7V versus RHE, but in [10, 27], the peak at about 0.4V vs. RHE is dominant, whereas in [4], the peak at about 0.5V is largest. The other difference lies in the fourth peak at 0.6V, suggested to be caused by OH adsorption [26]. This peak is far more pronounced in [4] than in [10, 27]. When planes vicinal to the Pt (100) surface are considered, the blank cyclic voltammetry shows a clear trend towards an increase in the peak at 0.4 V with smaller terrace size [4, 28], suggesting that this peak is related to one-dimensional ordered (100) step sites. Simultaneously, the peaks that were present at potentials higher than 0.42 V significantly reduced in size, suggesting that these features are linked to two-dimensional ordered (100) domains. [4] The vicinal

planes considered had (100) terraces and (111) steps, which remain unreconstructed after flame-annealing [34].

The role of flame-annealing and cooling atmosphere was previously demonstrated with Pt (111) in acid [35] and alkaline [36] media, where no visible difference in blank cyclic voltammetry was found, but the manner of electrode preparation did have a large effect on catalysis. Preliminary findings in our group [37] show that for Pt (100) the pretreatment has an effect on both blank CV and CO oxidation. Dependence of the peaks at 0.4 and 0.5 V vs. RHE on the pretreatment method was found, as well as the increase in CO stripping peak potential for hydrogen/argon or CO/argon cooled crystals compared to the argon cooled electrode.

A more detailed investigation into the features observed in the blank cyclic voltammetry, and their dependence on cooling atmosphere is reported in this communication. We use voltammetric techniques in correlation with the STM images of Kibler *et al.* in sulfuric acid [23] to interpret the features that arise in blank cyclic voltammetry of Pt (100) in alkaline media. Furthermore, we discuss various ways of pre-treating the electrode before immersion in the electrochemical cell, and show the effects on the blank CV and catalytic activity for oxidative stripping of carbon monoxide, hereafter referred to as CO stripping. From vacuum studies, it is known that CO forms different adsorbate structures on reconstructed Pt (100) compared to unreconstructed Pt (100). [21] Furthermore, in accordance with the recently published results on Pt (111) [38], we show that alkali-metal cations influence both the blank cyclic voltammetry of Pt (100), and the activity for CO stripping. Finally, we introduce anions and compare the results with Pt (533), which has terraces of (111) geometry with (100) steps, to conclusively assign the observed peaks in the blank CV to specific surface processes.

8.2 Materials and Methods

We used bead-type single crystals of platinum with a diameter of *ca.* 3 mm. They were prepared by flame annealing at a fixed position in a natural gas Bunsen burner, with an identical position and flame for each annealing, and controlled cooling in a cooling gas stream. When no carbon monoxide was present in the cooling gas, the electrode was immersed in water saturated with the cooling gas before being transferred to the electrochemical cell. With CO in the cooling gas stream, the electrode was covered with CO after cooling, and protection with a drop of water

was not necessary, as the electrode was already protected by the CO. The crystal was immersed in the electrolyte under potential control at 0.1 V versus RHE.
We used a Teflon cell of similar design to the one used before [38], with a Pt wire as the counter electrode. All experiments were performed with an Autolab PGSTAT 12 with a noise-reducing capacitor between the reference electrode and a second Pt counter electrode in the cell. The reference used was a calomel electrode, separated by a salt bridge from the main cell compartment. All potentials reported are converted to the pH independent reversible hydrogen electrode (RHE) scale.
The electrolytes were prepared by dissolving the selected hydroxides in 18.2 MΩ cm resistive Milli-Q water. $KOH{\cdot}xH_2O$ was obtained from Fluka; TRACEselect ≥99.995% trace metals basis (tmb). The NaOH and LiOH used were from Sigma-Aldrich; both pellets of 99.995% tmb. CsOH H_2O was also obtained from Sigma-Aldrich; 99.95% tmb, and finally KBr was used with a purity of 99.95% tmb, also from Sigma-Aldrich. All gases were of scientific grade (N5.5 or higher).

8.3 Results

8.3.1 Effect of electrode preparation method

To correlate our surfaces to the STM images by Kibler *et al.* [23], we used essentially the same methods of cooling the electrode after flame annealing, with the only difference that we substituted argon for N_2. Pure carbon monoxide (CO) was used, as well as pure hydrogen, to give as large a contrast with cooling in argon and air as possible. CO was adsorbed from solution for the electrodes, with the exception of the CO-cooled crystal, where the carbon monoxide was obviously present on the electrode when transferring to the cell. For the CO cooled crystal, CO stripping was performed with the CO present on the electrode from the cooling gas.
Figure 8.1A shows the blank cyclic voltammetries (CVs) of the same Pt (100) crystal in 0.1M KOH, when cooled in these alternate ways. The two most striking features are the peaks in the positive-going scan at 0.4 V and 0.48 V. In the negative-going scan they are mirrored by peaks at 0.46V and 0.38 V, thereby showing some modest irreversibility. The peak at 0.46V in the reverse scan is significantly smaller than the peak at 0.48V in the positive scan. An interesting observation is the dependence of these peaks on the cooling method. One observes

that the peaks at 0.38V and 0.4V are most pronounced when the electrode is cooled in argon or air; and the peaks at 0.46V and 0.48V are most pronounced when the electrode is cooled in hydrogen or CO. In fact, when the electrode is cooled in air, the pair of peaks at 0.46V and 0.48V completely disappears. The order in size of this peak is CO > H_2 >> Ar > air. A hydrogen-cooled Pt (100) shows a small peak at 0.4V, which is almost absent on the CO-cooled electrode. Furthermore, the current in the potential region from 0.3V to 0.5 V is higher for the H_2 cooled crystal than for the CO cooled crystal. At a potential of 0.3V, features corresponding to hydrogen adsorption on Pt (110) sites are visible for each preparation method. The next noticeable difference in the CVs can be seen at 0.3V in the negative-going scan, where a broad feature is visible when the electrode is cooled in hydrogen or CO, whereas this feature is absent after air or argon cooling. The third significant change is visible at 0.6V, where small peaks are visible for the H_2 and CO cooled electrode, but in the case of argon and air cooling only a broad region remains. Finally, the region negative of all the peaks, with a potential lower than 0.2V, shows a significant increase of current density in the order of CO < H_2 < Ar < air.

When the charge of the CV up to 0.53 V is analyzed, a value of 250 μC $cm_{geom.}^{-2}$ is found. This is 25% more than the charge for a monolayer of hydrogen on a flat Pt surface and can be explained by an excess of Pt atoms on the surface due to the lifting of the reconstruction. The reconstructed hex-phase is about 24% more densely packed than the unreconstructed surface. Upon cooling the crystal after annealing, small islands formed by the excess Pt atoms will arise on the surface due to the lifting of the reconstruction. [23] These islands may in turn increase the charge of the blank CV and explain why the value is higher than for a single monolayer on atomically flat Pt.

The CO stripping curves on the various electrodes are very different as well. Figure 8.1B shows the positive-going scan; and figure 8.1C the subsequent negative-going scan after CO has been stripped off. The shift in stripping peak potential (1B) is very noticeable, and increases in the order air < Ar < H_2 < CO. The charge of the CO stripping is equal for all methods of cooling, except for the air-cooled one, which has a 10% reduced charge. This is a slightly different result from what Rodriguez *et al.* found [37], and can be explained by the fact that their electrode was quenched after cooling in air until it was no longer glowing, and the electrode in our case was cooled in air to room temperature, thereby increasing the likelihood of contamination to adsorb on the electrode. Also, their method of quenching increases the amount of defects, which may explain their increased CO stripping charge. For all other methods of cooling described here, the CO stripping charge is

comparable to the results of Rodriguez *et al.* [37]. The second consecutive scan for all electrodes (shown in figure 8.1A as blanks) shows no sign of CO, indicating a clean, CO-free electrolyte. The negative-going scan, visible in 1C, is slightly different from the negative-going scan in the consecutive sweep (1A). At a potential of 0.27V, a large reductive peak is visible when the electrode is cooled in hydrogen or CO. The fact that this peak reduces in size upon cycling, compare for example with the second cycle in figure 8.1A, hints at a surface change. This peak is absent when the electrode is cooled in argon or air. Interestingly, this feature agrees with the (110) peaks mentioned before.

Next, the dependence of the surface state as a function of a hydrogen-argon cooling mixture was investigated. This mixture is commonly used in the flame annealing of single crystal electrodes. The results are depicted in figure 8.2. Similar to figure 8.1, part A of figure 8.2 shows the blank cyclic voltammetry (the second consecutive scan after CO stripping), B shows the CO stripping itself, and C the negative-going scan following the stripping curve. A range of ratios from Ar:H_2 6:1 through 1:2 was measured, though only curves corresponding to three ratios are shown. The black curve represents the electrode cooled in pure argon for comparison, and the green curve shows the pure H_2-cooled crystal. Blue, orange and red show the 5:1, 3:1 and 1:1 ratios of Ar:H_2, respectively. CO was adsorbed from the solution for electrodes cooled in this way, before any blank cyclic voltammetry was measured.

The first thing that is notable is the shift in peak potential of CO stripping, shown in figure 8.2B. The more hydrogen used in cooling, the more positive the CO stripping peak, up to a mixture of about 1:1, which resembles the pure hydrogen cooled electrode. When the blank CVs are compared (2A), three transitions are very distinct. First, the main peak at 0.48V gets smaller with less hydrogen in the cooling stream, and it shifts to lower potentials, becoming more reversible with the negative-going peak at 0.46V. Second, the feature slightly positive of 0.4V shifts negative to coincide in position with the peak observed at 0.4V on the Ar-cooled electrode, and increases slightly in size. And finally, in the negative-going scan, the feature at 0.3V decreases with decreasing hydrogen content in the cooling stream. Less distinct, but definitely noticeable is the decrease in the features at 0.6V with decreasing H_2 content. The reverse scan after CO stripping (2C) has a clear feature at 0.3V, where it can be seen that the pure hydrogen cooled electrode has a single peak, and the 1:1 cooled electrode has a shoulder slightly positive of the peak. When the mixture is made less hydrogen-rich, the feature changes completely to show the (110) peak at 0.27V and a peak at 0.38V that was also observed on air and argon cooled electrodes.

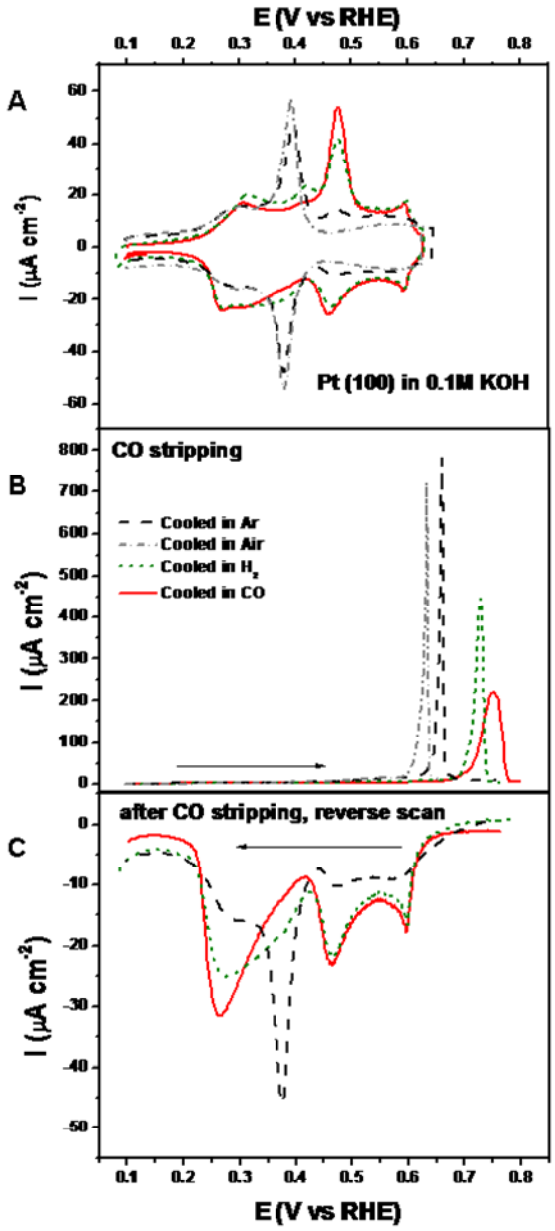

Figure 8.1. A. Blank cyclic voltammetry of Pt (100). The different curves represent Pt (100), cooled in pure Argon (black), pure hydrogen (green), pure CO (red) and air (grey). Part B shows the positive going scan CO stripping curve, and C the negative going scan. All scans were made in 0.1M KOH, with a scan rate of 20 mV s^{-1}.

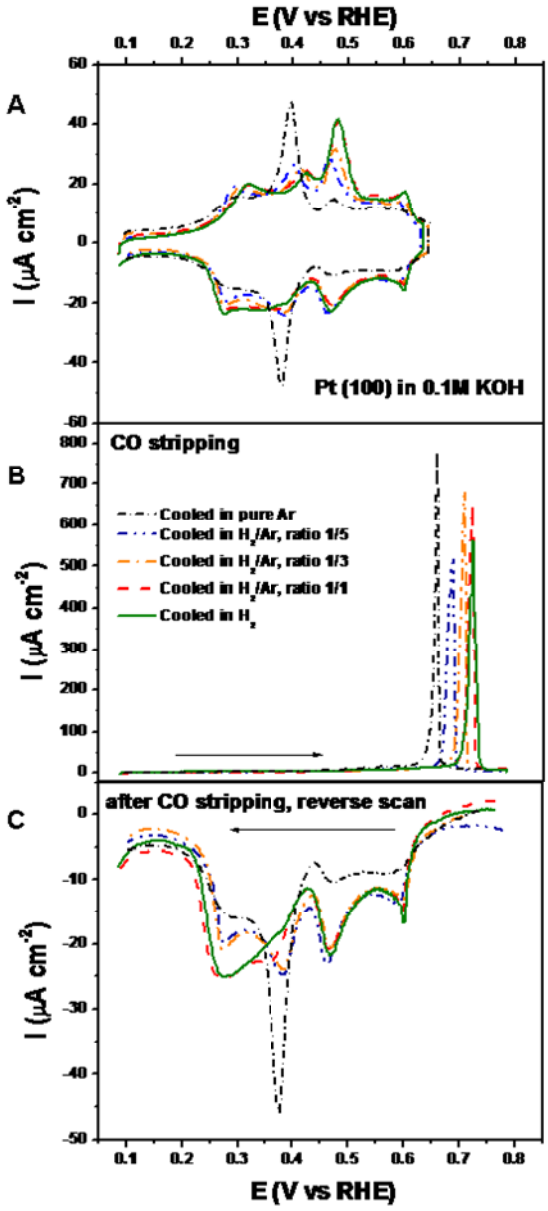

Figure 8.2. Dependence of blank cyclic voltammetry (A) and CO stripping (B in positive going scan, C in negative) on cooling method when using a mixture of Ar/H_2. All scans were made in 0.1 M KOH at 20 mV s^{-1}. The black line and grey line show reference voltammetries of Pt (100) cooled in argon and air, respectively. Blue (1/6), orange (1/3), red(1/1) and green (2/1) curves show an increasing order in (hydrogen/argon) content in the cooling gas flow.

Different CO to Ar ratios were applied as well, but the results (not shown graphically) were less clear-cut than for H_2:Ar cooled crystals. The trend was identical (higher CO stripping potential with increasing CO content in the cooling stream), but the reproducibility was more problematic, causing a wide scattering of peak potentials. This leads to the conclusion that when an electrode is cooled in a CO-containing inert gas stream, the amount of CO present is less critical than when cooled in a H_2:Ar gas stream; a stream containing small amounts of CO could lead to the same surface as when cooled in a high CO-content gas stream. In all CO-cooling experiments, however, one trend was clear: regardless of the CO-content in the cooling stream, the higher the CO stripping peak potential, the bigger, and at lower potential, the feature at around 0.28V in the negative-going scan.

8.3.2 Effect of potential cycling

The reason why CO stripping is performed before recording blank CVs can be deduced from figure 8.3. After cycling the electrode 5 times (orange curve) the peak at 0.48V has shifted slightly negative, and is reduced in height. This trend continues when the electrode is cycled more, as shown by the red curve obtained after 25 blank cycles and the blue curve obtained after 55 blank cycles. The blank cyclic voltammograms, shown in figure 8.3A, show the consecutive cycles after CO stripping, the cycles in-between were made to an upper limit of 0.6V vs. RHE. Simultaneously with the peak decrease at 0.48V, the feature at 0.4V increases with increasing numbers of cycles.

The CO stripping peak potential (figure 8.3B) shifts to lower potentials with increasing numbers of cycles, until it is stable for heavily cycled (more than 50 cycles) Pt (100). Combined with the obvious broadening of the peak, this is a clear indication that the surface morphology has changed. In the negative-going scan, the most negative features are shifting positive with increasing numbers of cycles. The results shown in the figure were made without losing potential control on the electrode, and in the same electrolyte. To exclude the effects of carbonate, formed while saturating the electrode with CO and subsequent oxidation, a series of blank cyclic voltammograms was also made without intermittent CO-stripping. These CVs show the same trend as the ones shown in figure 8.3A. Furthermore, scanning the electrode at lower scan rate, for example at 5 mV s^{-1}, will have a similar effect as many cycles at higher scan rate.

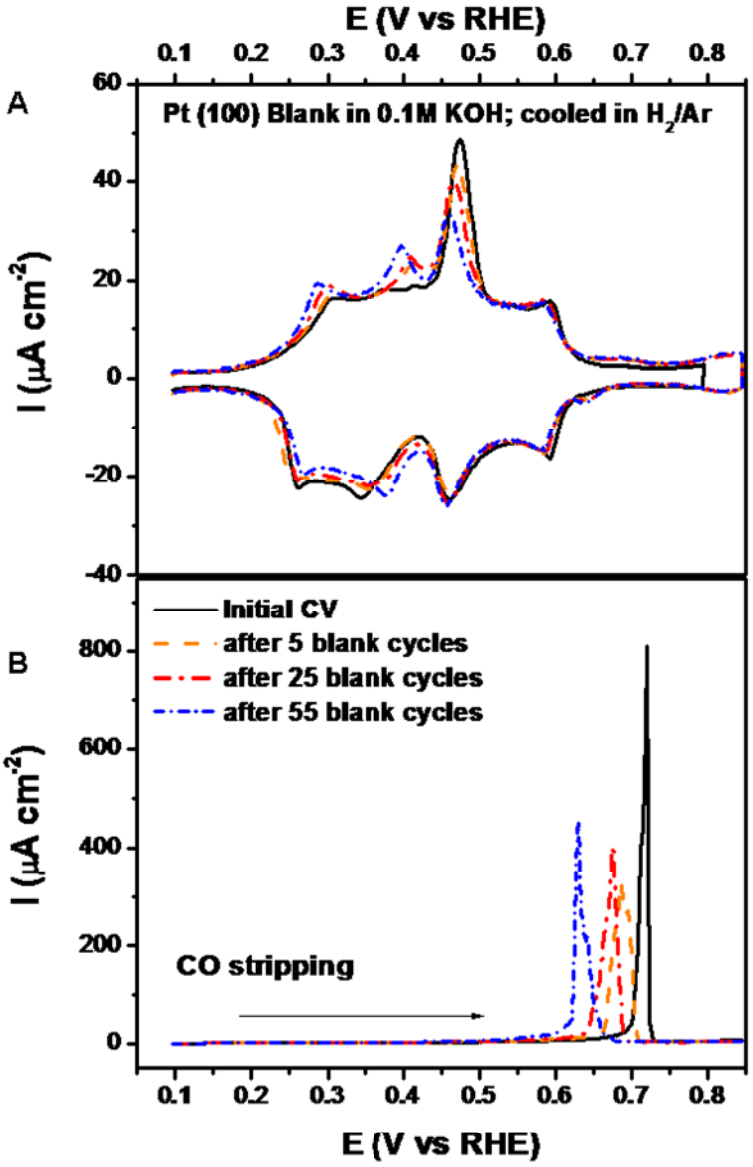

Figure 8.3. The effect of cycling in argon-purged solution up to a potential of 0.6V vs. RHE. In part A, the black graph shows the initial blank CV of H_2/Ar (1/3) cooled Pt (100), orange (5 cycles), red (25 cycles) and blue (55 cycles) show the voltammetries after their respective CO stripping (shown in part B). The electrode was cycled up to 0.6V in between the CO stripping curves. All scans were made in 0.1 M KOH at 20 mV s^{-1}.

8.3.3 Cation and Anion effects

Finally, the effects of cations and anions on the blank CV and CO stripping on Pt (100) were investigated. The results are shown in figure 8.4 (cation effect) and figure 8.5 (bromide effect). The blank cyclic voltammograms for the different metal hydroxide electrolytes (figure 8.4A) show three interesting trends. First of all, the most obvious of the three, is the influence on the pair of peaks with the highest potential of 0.6V. This peak sharpens when the cation is changed from Cs → K → Na → Li. In LiOH this gives what we interpret as a very small double-layer region between H desorption and OH adsorption, which normally is not observed on Pt (100). The second and third effects are coupled. The main peak at 0.48V, as well as the feature in the negative going scan at 0.28V, decreases in intensity when the cation is changed from Li to Cs. The feature at 0.28V is even more pronounced with the smaller cations in the negative-going scan after CO stripping (figure 8.4C). For lithium hydroxide this peak remains nearly identical in the consecutive blank scan (shown in part A). The CO stripping peak shows the trend that the peak potential decreases in the order $K \approx Cs > Na > Li$; the inset in figure 8.4B shows the peak potentials plotted for the various cations, with their standard deviations over 4 independent measurements.

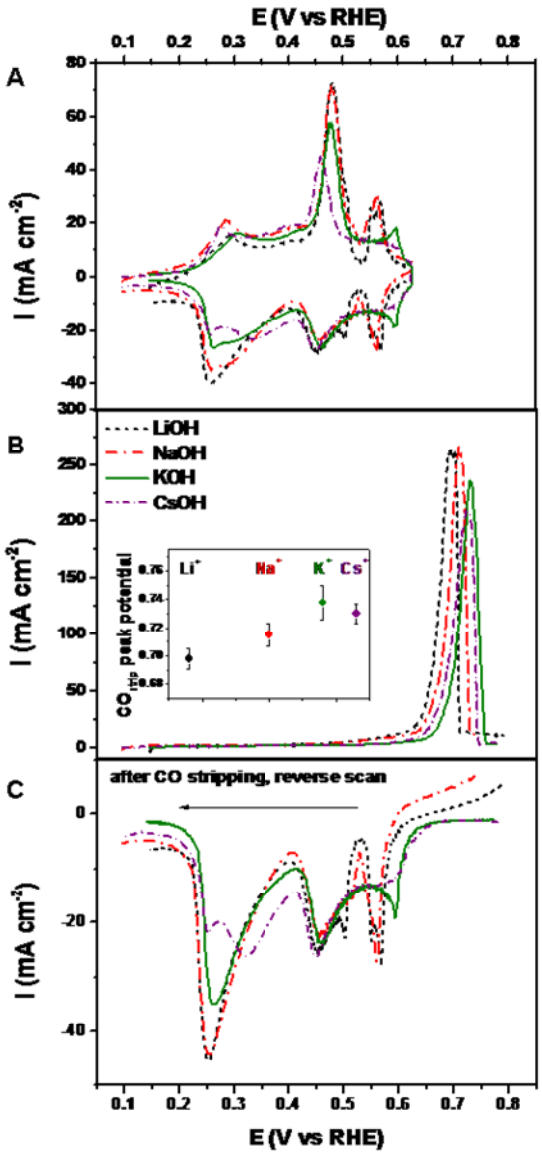

Figure 8.4. Effect of the alkali-metal cation. Part A shows the blank cyclic voltammetries, and B and C show CO stripping in positive, and negative-going scan, respectively. The inset in part B shows the peak potential as function of the cation, with the error bars representing the standard deviation in 4 independent measurements. All scans were made with the electrode cooled in 1:1 CO:Ar, then transferred to 0.1M MOH with M = Li (black) Na (red), K (green) and Cs (purple). Scans were made with 20 mV s^{-1}.

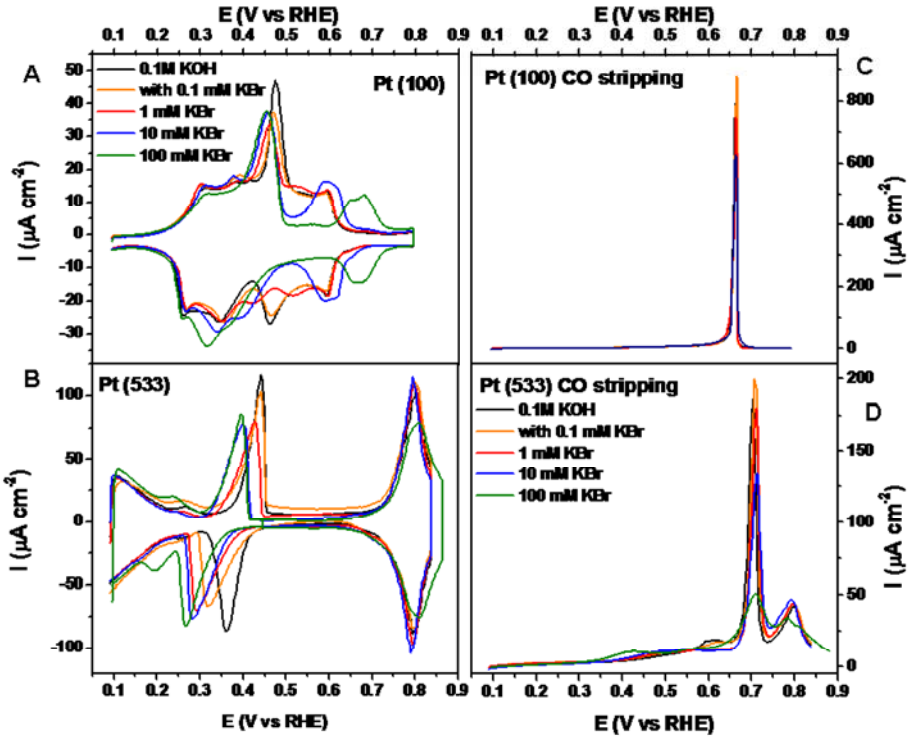

Figure 8.5. Effect of bromide on Pt (100) (A and C) and Pt (533) (B and D) A and B show the blank cyclic voltammetry, C and D illustrate CO stripping. The black line represents the blank CV in 0.1M KOH; orange, red, blue and green show the curves with an order of magnitude increase in bromide concentration each, starting at $1 \cdot 10^{-4}$ M. Blank scans were made with a scan rate of 50 mV s^{-1}, CO stripping was performed at 20 mV s^{-1}. The electrodes were cooled in 3:1 Ar:H_2 after annealing.

The effect of anions (bromide) on the blank CV is shown in figure 8.5. Part A shows the effect on H_2:Ar cooled Pt (100). The most striking effect is the change in OH adsorption features (peak at 0.6V). For less than 1 mM KBr, this peak remains essentially unaffected, but when the concentration is consecutively increased it shifts to much more positive potentials, giving rise to an extended "double-layer" region in which we assume the electrode to be covered with a Br-adlayer. In the negative-going scan, the peak at 0.46V seems to split. This is best visible in the 1 mM voltammetry, where two peaks are evident at 0.42V and 0.52V instead of a single one. For higher concentrations of bromide, these two peaks seem to shift even further apart; the more positive one coinciding with the OH peak, the most negative one visible as a shoulder on the peak at about 0.32V. The other feature in the negative-going scan at 0.35V is that it shifts steadily more negative with

increasing anion concentration. This is coupled to the positive-going scan, where the main peak at 0.48V also shifts negative with increasing bromide concentration. This trend is mirrored in figure 8.5B on Pt (533) (which has 4 atom wide (111) terraces and (100)-steps), where the features of hydrogen adsorption associated with the (100) step sites shift steadily negative when the bromide concentration is increased. This shows that these features are most definitely connected to hydrogen ads- and desorption. In contrast to Pt (100), the change on the OH adsorption on (111) terraces on Pt (533) is minimal, most likely due to the lower affinity of anions to (111) sites in alkaline media (see also [39]), causing the OH adsorption on (111) sites to be less influenced by anion coadsorption.

The effect of anions on CO stripping is illustrated in figure 8.5C and D for Pt (100) and Pt (533) respectively. For Pt (100) the only effect is that the stripping peak current gets lower, and that the whole feature broadens slightly. The total charge of CO stripping remains equal for all concentrations of bromide. On Pt (533) the effect is slightly more pronounced. The pre-oxidation wave (0.35-0.65V) starts at lower potentials for increased bromide concentration, while the main peak increases slightly in potential. The total CO stripping charge remains constant at about 340 μC cm^{-2} until the concentration bromide exceeds 10 mM; then it diminishes to about 310μC cm^{-2} for the Br^- concentration of 0.1M. This is likely due to competitive adsorption between Br^- and CO. As a reference, the CO stripping curves in bromide containing electrolyte for Pt (111) are shown in figure 8.6. Here can be seen that the bromide has little influence on the main peak potential. The onset of the pre-oxidation peaks remains the same for increased concentrations of bromide, but the charge of the pre-oxidation features decreases significantly. This once again shows that in alkaline media, bromide competes for the lower coordinated sites, but not for the (111) terraces.

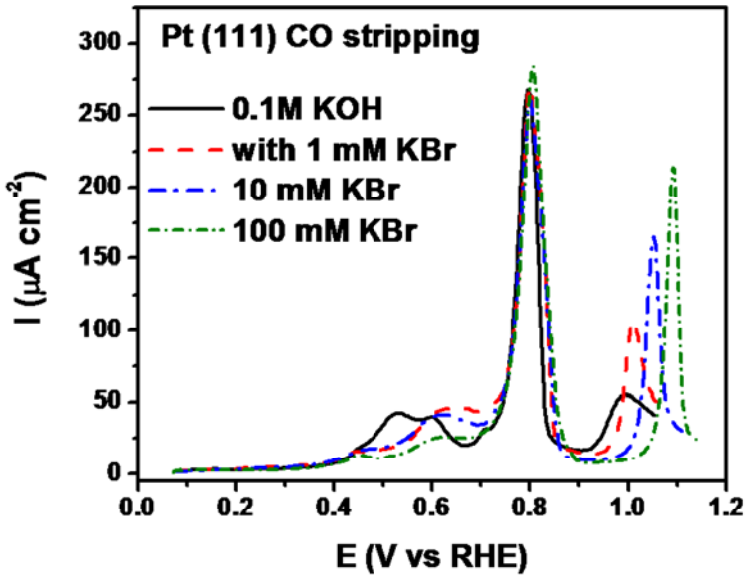

Figure 8.6. CO stripping on Pt (111) (with defects) in 0.1M KOH with increasing concentrations of bromide. The black line shows the CO stripping without bromides, the red, blue and green lines with 1 mM, 10 mM and 0.1 M KBr, respectively. Scan rate 50 mVs^{-1}. The electrode was cooled in 3:1 Ar:H_2 after annealing.

8.4 Discussion

In this section we will summarize our interpretation of the influence of surface preparation on the cyclic voltammetry and CO stripping. The pair of peaks at the lowest potentials (0.3 V) has been attributed to Pt (110)-type defects, due to their position which agrees with the hydrogen adsorption features on Pt (110). [4, 26] The next pair of peaks at 0.38V and 0.4V is most pronounced when the electrode is cooled without CO or hydrogen present (figure 8.1), and can be attributed to a mixture of defect sites and low-range order (100) sites. This is evident from the observation that these peaks grow when cooled in air, which is known to increase defects [23], and that they increase on the unreconstructed surfaces, vicinal to Pt (100) [4, 34]. Interestingly, these peaks also seem to be most pronounced for the argon-cooled surface, which was shown to be reconstructed in the electrolyte [23]. Regardless of their exact structural origin, they clearly do not represent long-range Pt (100) terraces.

Such long-range (100) terraces exhibit hydrogen adsorption/desorption features in two large peaks, which are separated significantly. In the positive-going scan, the main peak at 0.48V can be seen to diminish during cycling, and with less perfect cooling methods, thereby indicating its relationship to terraces of long-range order. This is coupled with the peak at 0.28V in the negative-going scan, which diminishes when the main peak at 0.48V grows smaller. There are two possible explanations for the diminishing of these peaks during cycling. First of all, it has been shown in figure 8.3 that cycling introduces defects, resulting in a reduction of long-range order. Secondly, hydrogen adsorption processes have been shown to lift a reconstructed surface [24, 25]. In our case, however, the features change most for CO and H_2 cooled surfaces, which were shown to be unreconstructed in the first place. [7] This reinforces our belief that the features at 0.48V in the positive-going scan and at 0.28V in the negative-going are very sensitive to the long-range Pt (100) order, and that both cooling in a non-reductive atmosphere and potential-cycling in an electrochemical cell reduce significantly the long-range order of a Pt (100) crystal.

We believe the nature of the processes that give rise to these features is ads- and desorption of hydrogen, combined with cation-stabilized adsorption of OH, similar to the model in [38]. As can be seen in figures 5A and 6A, the two features are dependent on the nature of the cation, as well as the bromide concentration, which is a clear indication that there is an anionic contribution to both features. The irreversibility that can be seen in the blank CV is most likely caused by the stability of the adsorbed anions and OH on the well-ordered surface. On less well-ordered surfaces (such as after many blank cycles, see figure 3), the interaction of these anionic species may be weaker, causing the CV to become more reversible with decreasing long-range order.

The final set of peaks that is visible in the blank cyclic voltammetry, centered at about 0.55-0.6V, can be attributed to OH adsorption. The fact that they shift positive when bromide adsorption is blocking the surface for OH_{ads} (figure 8.5), and that they sharpen when a more OH-interacting cation is used (figure 8.4) supports this conclusion. This peak-sharpening in itself can be explained by the model in [38], when one considers the (hydrated) metal cation to be quasi-specifically adsorbed through the OH_{ads} on the surface. Lithium, which has the strongest interaction with OH_{ads}, shows the sharpest peak, and cesium, which has the weakest interaction with OH_{ads}, exhibits the broadest feature.

Our results illustrate that it is important to prepare the crystal in a correct way. As figure 8.1B and figure 8.2B show, the preparation method can influence catalytic

properties dramatically . When cooling the crystal in a mixture of hydrogen and argon, as is usual in electrochemistry, a higher concentration of hydrogen (at least 50% hydrogen content in the cooling stream) is preferred to prepare a surface consisting of large well-ordered Pt (100) terraces. Better yet for long-range order is the inclusion of carbon monoxide in the cooling stream. Furthermore, as is evident from figure 8.3, making blank CVs is detrimental to the long-range order, and worse still, it will introduce defects as visible from the CO stripping in figure 8.3B. CO stripping in alkaline media is a structure-sensitive process [40], and defect sites have been shown to have the lowest peak potential for CO stripping. Therefore, when the peak potential reduces, and the peak broadens, as in figure 8.3B, it illustrates the formation of defects on the surface. Interestingly, the CO stripping peak potential after cycling the electrode for a long time is nearly identical to the CO stripping peak potential for the air-cooled electrode (figure 8.1B), reinforcing previous findings on the highly defected nature of the air-cooled crystal [23].

The cation effect on CO stripping is very clear: in the sequence Li < Na < K = Cs the stripping peak potential increases. The stronger the interaction of the metal-cation with OH, the stronger it will quasi-specifically adsorb on the surface. This also means that the stronger the M-OH interaction, the sooner it will be able to initiate the CO electro-oxidation through the Langmuir-Hinshelwood mechanism. The M-OH interaction increasing in the range Cs < K < Na < Li is exactly opposite of the CO stripping peak trend, which supports our conclusion of a higher affinity for CO stripping with increasing M-OH interaction. It is interesting to note that in a previous result on Pt (111) [38], the onset of methanol oxidation showed the same trend as the CO stripping in this work. The same result was obtained in our group for CO stripping from a Pt (111) surface. [41] Bromide seems to have little influence on the catalytic activity of Pt (100) towards CO stripping, but does have a profound effect on the adsorption processes which are visible in the blank cyclic voltammetry. Bromide competitively adsorbs with protons, shifting the adsorption features due to H_{upd} to slightly more negative potentials. Higher concentrations of bromide also delay surface oxidation, shifting the OH_{ad} feature of the (100) terraces more positive. In order to more accurately assign the peaks in the blank CV, Pt (533) was measured as well. The negative shift of the (100) step-related H_{upd} peak is mirrored on that surface, but anions do not have the same effect on the reversible OH_{ad} peak of the (111) terraces at 0.8V. This clearly shows the stronger interaction of bromides in alkaline media with the Pt (100) surface compared to Pt (111). For the catalytic activity towards the electro-oxidative stripping of CO the effect is minimal. It is interesting to note that when there are fewer (100) sites available,

such as on Pt (533), there is a bigger difference in CO stripping for the different Br^- concentrations. Likely Br^- is competing with active sites for the oxidation of adsorbed CO, which is more evident when fewer sites are available. On Pt (111), there is no difference in CO stripping main peak potential or charge with increasing bromide concentrations, but a significant effect on the pre-oxidation wave due to lower-coordinated defect sites. This indicates strongly that the difference in CO stripping main peak potential observed on Pt (533) must be due to the (100) sites present.

8.5 Conclusion

The mixture of gases in which the Pt (100) crystal is cooled after flame-annealing is critical to the quality of the surface structure. Blank cyclic voltammetry in alkaline media is very sensitive to the manner of surface preparation. Cooling in air and argon causes the surface to have far less long-range 1x1 order. Cooling in hydrogen-containing argon will give a much better surface, but the amount of hydrogen is important. The more hydrogen (up to 50%) present, the better the surface. The best preparation method to obtain long-range (100) islands is by cooling in a mixture of carbon monoxide and argon.

Differences in the literature on the blank cyclic voltammetry of Pt (100) are caused by a combination of this annealing methodology, the influence of cycling, as well as the difference in cation used. The OH_{ads} features of Pt (100) become sharper with increasing M-OH interaction in the order Cs < K < Na < Li. The CO stripping onset and peak position shifts in exactly the opposite order, with CO stripping in lithium having the lowest onset and peak potential.

Finally, the addition of bromides has the effect on the blank cyclic voltammetry that the peaks attributed to hydrogen adsorption and desorption shift to lower potentials with increasing bromide concentration, and the OH-peaks shift positive. At concentrations of $1 \cdot 10^{-4}$ M and higher, a "double-layer" becomes visible, where the H_{ads} and OH_{ads} processes are clearly separated by a region on which bromide is adsorbed on the electrode. There appears to be competition of bromide adsorption with CO oxidation for (100) sites, which is evident from the difference in CO stripping curves on Pt (533). This effect is not observed on Pt (100), most likely due to the increased availability of these sites. Anion adsorption on Pt (111) in alkaline media is weak, and there such a competition is not observed.

References

[1] K. Itaya, Progress in Surface Science. 58 (1998) 121.
[2] G. Jerkiewicz, Solid-Liquid Electrochemical Interfaces. 656 (1997) 1.
[3] A. A. Gewirth and B. K. Niece, Chemical Reviews. 97 (1997) 1129.
[4] F. J. Vidal-Iglesias, N. Garcia-Araez, V. Montiel, J. M. Feliu, and A. Aldaz, Electrochemistry Communications. 5 (2003) 22.
[5] V. Rosca, G. L. Beltramo, and M. T. M. Koper, Journal of Physical Chemistry B. 108 (2004) 8294.
[6] L. Vattuone, L. Savio, and M. Rocca, Surface Science Reports. 63 (2008) 101.
[7] M. Brandt, G. Zagatta, N. Bowering, and U. Heinzmann, Surface Science. 385 (1997) 346.
[8] H. P. Bonzel, G. Broden, and G. Pirug, Journal of Catalysis. 53 (1978) 96.
[9] W. K. Offermans, A. P. J. Jansen, R. A. van Santen, G. Novell-Leruth, J. M. Ricart, and J. Perez-Ramirez, Journal of Physical Chemistry C. 111 (2007) 17551.
[10] T. J. Schmidt, P. N. Ross, and N. M. Markovic, Journal of Physical Chemistry B. 105 (2001) 12082.
[11] R. A. Van Santen, Accounts of Chemical Research. 42 (2008) 57.
[12] V. Rosca and M. T. M. Koper, Physical Chemistry Chemical Physics. 8 (2006) 2513.
[13] M. A. Vanhove, R. J. Koestner, P. C. Stair, J. P. Biberian, L. L. Kesmodel, I. Bartos, and G. A. Somorjai, Surface Science. 103 (1981) 189.
[14] M. A. Vanhove, R. J. Koestner, P. C. Stair, J. P. Biberian, L. L. Kesmodel, I. Bartos, and G. A. Somorjai, Surface Science. 103 (1981) 218.
[15] D. L. Abernathy, D. Gibbs, G. Grubel, K. G. Huang, S. G. J. Mochrie, A. R. Sandy, and D. M. Zehner, Surface Science. 283 (1993) 260.
[16] D. L. Abernathy, S. G. J. Mochrie, D. M. Zehner, G. Grubel, and D. Gibbs, Physical Review Letters. 69 (1992) 941.
[17] D. L. Abernathy, S. G. J. Mochrie, D. M. Zehner, G. Grubel, and D. Gibbs, Physical Review B. 45 (1992) 9272.
[18] D. Gibbs, G. Grubel, D. M. Zehner, D. L. Abernathy, and S. G. J. Mochrie, Physical Review Letters. 67 (1991) 3117.
[19] P. Heilmann, K. Heinz, and K. Muller, Surface Science. 83 (1979) 487.
[20] J. Clavilier, R. Durand, G. Guinet, and R. Faure, Journal of Electroanalytical Chemistry. 127 (1981) 281.
[21] G. Broden, G. Pirug, and H. P. Bonzel, Surface Science. 72 (1978) 45.
[22] J. Radnik, F. Gitmans, B. Pennemann, K. Oster, and K. Wandelt, Surface Science. 287 (1993) 330.
[23] L. A. Kibler, A. Cuesta, M. Kleinert, and D. M. Kolb, Journal of Electroanalytical Chemistry. 484 (2000) 73.
[24] A. Al-Akl, G. A. Attard, R. Price, and B. Timothy, Journal of Electroanalytical Chemistry. 467 (1999) 60.
[25] K. Wu and M. S. Zei, Surface Science. 415 (1998) 212.
[26] N. M. Markovic, H. A. Gasteiger, and P. N. Ross, Journal of Physical Chemistry. 100 (1996) 6715.
[27] A. V. Tripkovic, K. D. Popovic, J. D. Momcilovic, and D. M. Drazic, Journal of Electroanalytical Chemistry. 448 (1998) 173.
[28] N. Furuya and M. Shibata, Journal of Electroanalytical Chemistry. 467 (1999) 85.

[29] T. J. Schmidt, P. N. Ross, and N. M. Markovic, Journal of Electroanalytical Chemistry. 524-525 (2002) 252.
[30] A. Rodes, V. Climent, J. M. Orts, J. M. Perez, and A. Aldaz, Electrochimica Acta. 44 (1998) 1077.
[31] E. Morallon, J. L. Vazquez, and A. Aldaz, Journal of Electroanalytical Chemistry. 288 (1990) 217.
[32] J. H. Barber and B. E. Conway, Journal of Electroanalytical Chemistry. 461 (1999) 80.
[33] F. J. Vidal-Iglesias, J. Solla-Gullon, V. Montiel, J. M. Feliu, and A. Aldaz, Journal of Physical Chemistry B. 109 (2005) 12914.
[34] N. Garcia-Araez, V. Climent, E. Herrero, and J. M. Feliu, Surface Science. 560 (2004) 269.
[35] N. P. Lebedeva, M. T. M. Koper, J. M. Feliu, and R. A. van Santen, Electrochemistry Communications. 2 (2000) 487.
[36] G. Garcia, P. Rodriguez, V. Rosca, and M. T. M. Koper, Langmuir. 25 (2009) 13661.
[37] P. Rodriguez, G. Garcia, E. Herrero, J. M. Feliu, and M. T. M. Koper, in preparation, to be submitted. (2010).
[38] D. Strmcnik, K. Kodama, D. van der Vliet, J. Greeley, V. R. Stamenkovic, and N. M. Markovic, Nature Chemistry. 1 (2009) 466.
[39] R. Gisbert, G. García, and M. T. M. Koper, Electrochimica Acta. In Press, Corrected Proof.
[40] G. Garcia and M. T. M. Koper, Physical Chemistry Chemical Physics. 10 (2008) 3802.
[41] C. Stoffelsma and M. T. M. Koper, In preparation.